AIP | Applied Physics Letters

Nanophotonic front electrodes for perovskite solar cells

Ulrich Wilhelm Paetzold, Weiming Qiu, Friedhelm Finger, Jef Poortmans, and David Cheyns

Citation: Applied Physics Letters **106**, 173101 (2015); doi: 10.1063/1.4918751
View online: http://dx.doi.org/10.1063/1.4918751
View Table of Contents: http://scitation.aip.org/content/aip/journal/apl/106/17?ver=pdfcov
Published by the AIP Publishing

Nanophotonic front electrodes for perovskite solar cells

Ulrich Wilhelm Paetzold,[1,2,a)] Weiming Qiu,[1] Friedhelm Finger,[2] Jef Poortmans,[1,3,4] and David Cheyns[1]
[1]*IMEC v.z.w., Kapeldreef 75, 3001 Leuven, Belgium*
[2]*IEK5-Photovoltaik, Forschungszentrum Juelich GmbH, D-52425 Juelich, Germany*
[3]*Katholieke Universiteit Leuven, ESAT-Electa, Kardinaal Mercierlaan, 3001 Leuven, Belgium*
[4]*Hasselt University, Wetenschapspark 1, 3590 Diepenbeek, Belgium*

(Received 5 February 2015; accepted 10 April 2015; published online 27 April 2015)

In less than 3 years' time, a vast progress in power conversion efficiencies of organometal halide perovskite solar cells has been achieved by optimization of the device architecture, charge transport layers, and interfaces. A further increase in these efficiencies is expected from an improvement in the optical properties via anti-reflection coatings and nanophotonic light management concepts. In this contribution, we report on the development and implementation of a nanophotonic front electrode for perovskite solar cells. The nanostructures were replicated via the versatile and large-area compatible UV-nanoimprint lithography. The shallow design of the used transparent and conductive nanostructures enabled easy integration into our solution-based baseline process. Prototype methylammonium lead iodide perovskite solar cells show an improvement of 5% in short-circuit current density and an improvement from 9.6% to 9.9% in power conversion efficiency compared to the flat reference device. © *2015 AIP Publishing LLC*.
[http://dx.doi.org/10.1063/1.4918751]

The enormous potential and recent vast development of organometal halide perovskite solar cells has triggered an unprecedented fast progress of its power conversion efficiencies (η). Today, less than 3 years after the first reported solid state perovskite solar cell[1] a record efficiency of 20.1%[2] has been certified and several groups have reported efficiencies above 17%.[3,4] The current key challenges of perovskite solar cells are the apparent uncertainties about the stability of the devices,[5–7] the discrepancies in measuring routines due to hysteresis,[8,9] and the difficulties in replacing the toxic heavy metal lead.[10,11] The promise of perovskite solar cells is founded in their close to optimal combination of electrical and optical material properties. Free carrier diffusion lengths from 100 nm (Refs. 12 and 13) up to 1 μm (Ref. 13) have been reported for the current work-horse materials, methylammonium lead iodide perovskite ($CH_3NH_3PbI_3$) and the partially chlorine-substituted *mixed halide* perovskite ($CH_3NH_3PbI_{3-X}Cl_X$). In addition, the material shows a sharp optical absorption edge at wavelengths of 800 nm (i.e., 1.55 eV) with absorption depths below 350 nm (for $\lambda < 750$ nm).[14] Since the combination of these material properties allows for optically thick layers ($\geq$350 nm) in combination with close to optimal charge carrier collection, the first attention in the development of perovskite solar cells was directed towards the optimization[3,15–18] of the charge carriers dynamics in the device architecture,[3,7,13,15–23] in the charge transport layers,[12,24,25] and in the interfaces.[4,26] However, in order to further improve the efficiencies, the optical aspects of organometal halide perovskite solar cells need optimization. The reflection at the air/substrate interface is around 4% and additional reflection and parasitic absorption losses are apparent at the transparent front contact. While a broad range of anti-reflection coatings for the front side of transparent glass and plastic substrates have been explored,[27] research on nanophotonic transparent front electrodes for perovskite solar cells for improved light incoupling is lacking. Such nanostructured electrodes are intended

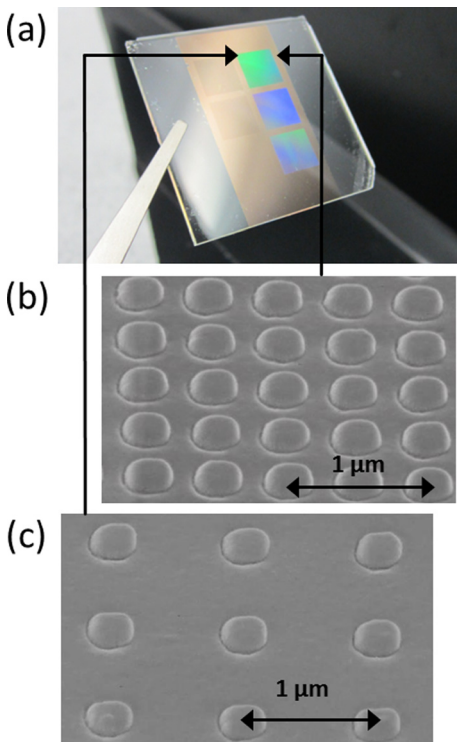

FIG. 1. Nanophotonic ITO front electrodes for application in perovskite thin-film solar cells. (a) A photograph of the ITO front electrode on the glass substrate. The colored haze depicts the light diffraction of the nanopatterned regions of the electrode. Scanning electron microscopy (SEM) image of the surface topography of the nanopatterned ITO front electrode with a period of (b) 500 nm and (c) 1000 nm.

[a)]Author to whom correspondence should be addressed. Electronic mail: ulrich.w.paetzold.ext@imec.be

to reduce reflection at both interfaces of the front electrode. Moreover, they can be used to improve the light-trapping, i.e., increase the optical path length in the photo-active material. Such nanophotonic transparent front electrodes have already been researched and prototyped for a number of other solar cells, such as organic based PV,[28–30] thin-film silicon,[31,32] GaAs (Ref. 33), and crystalline silicon.[34,35] In this contribution, we report on the prototyping and application of transparent nanophotonic front electrodes for improved light incoupling in perovskite solar cells.

The nanophotonic front electrode was prepared by nanopatterning a transparent glass-like resist on a plane glass substrate ($3 \times 3\,cm^2$). With a soft-polymer mold and a UV-nanoimprint process, periodic nanopatterns were transferred into the transparent resist that hardens at intense UV exposure (details on the nanoimprint process are described in the supplemental material[36] well as the literature[37,38]). A 125 nm thick indium-tin-oxide (ITO) layer was then sputtered onto the resist, forming the front electrode. The nanopatterned regions exhibit areas of $0.5 \times 0.5\,cm^2$ and periods ranging from 1200 nm to 500 nm. In contrast to the flat reference, light diffraction at periodic nanopatterns causes spectral selective redirection of light that can be observed by eye (shown in Figure 1(a)). Due to the moderate conformal growth of the sputtered ITO, the rectangular nanostructures at the surface of the UV-nanoimprinted resist (80 nm height and 300 nm width) reveal a semi-ellipsoidal shape (around 80 nm height and 320 nm width) at the ITO surface (see Figures 1(b) and 1(c)).

A methylammonium lead iodide perovskite solar cell was fabricated on top of the ITO front electrode. Since our substrate holds both nanopatterned and flat regions, it was possible to process both nanopatterned and reference devices in parallel and on the same substrate, i.e., using the same sputtered ITO material quality and layer thickness.[36] Moreover, our experiments ensure optimal comparability of the device architecture and material compositions, which is otherwise difficult to achieve for solution-processed layers. In Figure 2(a), a photograph of the entire device is shown. Five areas of $0.5 \times 0.5\,cm^2$ with decreasing brightness indicate the regions of the nanopatterns at the ITO front electrode. Some of the nanopatterns show a colored haze due to light diffraction at the two-dimensional nanopattern of the front electrode. The solar cells layer sequence was deposited onto these electrodes in the conventional device architecture, with the hole transport layer at the front electrode and the electron transport layer at the Al back electrode (layer sequence in Figure 2(b)). The device architecture presented here has been proposed before in literature by Bai *et al.*[39] A

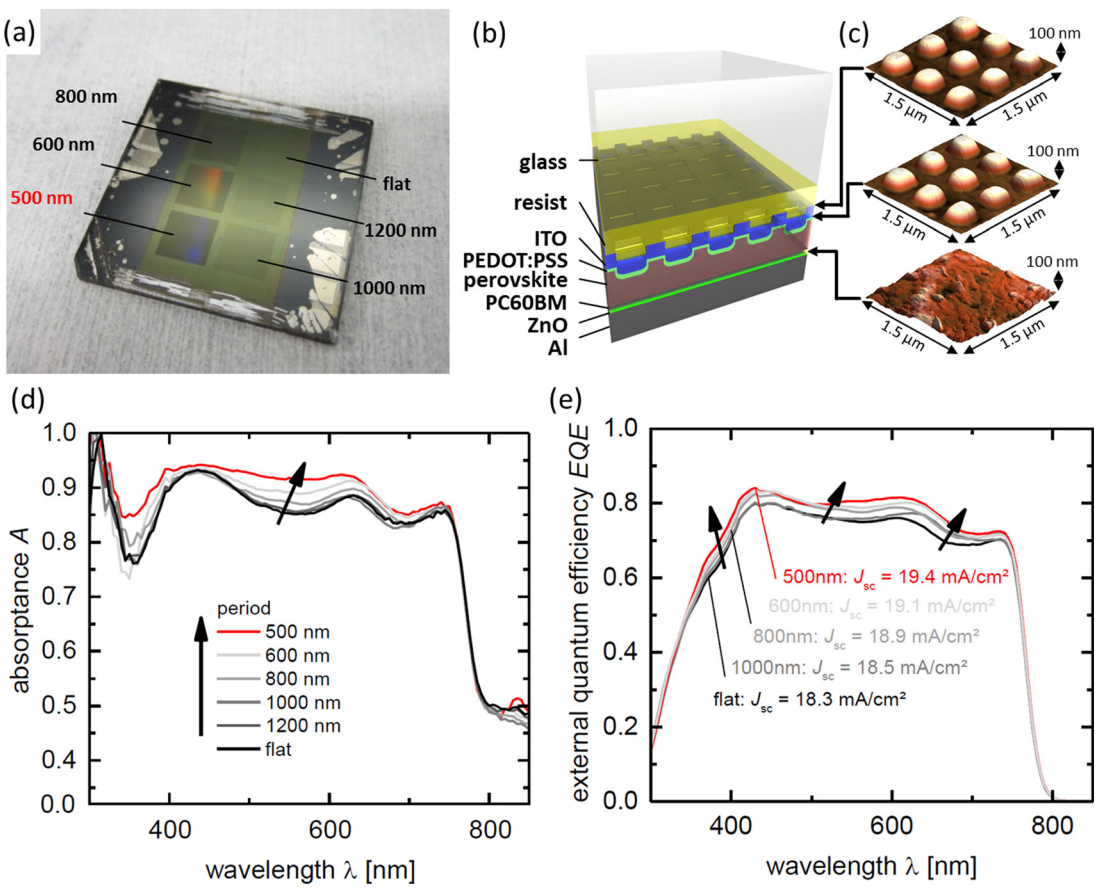

FIG. 2. Prototype methylammonium lead iodide solar cell. (a) A photography of the substrate from the front side. The five areas with decreased brightness indicate the regions of the nanopatterns of the ITO front electrode. For the 500, 600, and 800 nm patterns, light diffraction is apparent by a colored haze. (b) A schematic illustration of the nanopatterned perovskite solar cell. (c) Images of atomic force microscopy measurements of the nanopatterned resist, the nanopatterned resist covered with ITO, and the rear side of the perovskite solar cell. (d) The absorptance *A* and (e) the external quantum efficiency *EQE* of the methylammonium lead iodide solar cells with nanophotonic electrodes compared to solar cells deposited on the flat reference electrode. The period of the nanopattern is varied from 500 nm to 1200 nm.

spin-coated poly(3,4-ethylenedioxythiophene):poly(4-styrenesulfonate) (PEDOT:PSS) layer acts as hole transport layer in contact with the ITO front electrode. The photoactive methylammonium lead iodide perovskite $CH_3NH_3PbI_3Cl$ layer was prepared by annealing a "pristine" spin-coated precursor solution ($CH_3NH_3PbI_{3-X}Cl_X$). A spin-coated [6,6]-phenyl C60-butyric acid methyl ester ($PC_{60}BM$) and a spin-coated zinc oxide establish the bilayer-structured electron transporting layer. Finally, the reflective Al back electrode was deposited through a shadow mask defining the cell area (approximately 15 mm^2). More details on the processing conditions and composition of the applied solutions are presented in the supplemental material.[36] The thickness of the perovskite absorber layer was determined by profilometer measurements to 320 nm. The conformity of the ITO deposition on the nanopatterned substrates was investigated with atomic force microscopy measurements (Figure 2(c)). It is shown that the front electrode is nanostructured but the back electrode is flat. Since the photoactive perovskite layer is significantly thicker than the nanostructure at the front electrode, the nanopattern is not apparent at the back electrode. The combination of $PC_{60}BM$ and ZnO layers is of particular importance to our device architecture. This double layered electron transport structure fills the cavities existing in the methylammonium lead iodide perovskite layer after formation of the crystallites, while a low resistive contact with the cathode is attained with the ZnO.

The photograph in Figure 2(a) reveals that absorptance of incident light is increased for the solar cells deposited on the nanopatterned front electrodes compared to the flat reference. In order to quantify this observation we show the spectral resolved absorptance of the solar cells deposited on the nanophotonic front electrodes with periods ranging from 1200 nm to 500 nm in Figure 2(d). With decreasing period, the absorptance in the entire wavelength range is enhanced. This enhancement is attributed to a decreased light reflection and increased light transmission at the nanostructured ITO front electrode and the adjacent nanostructured layers. The cause of this decrease reflection and increased transmission lies in the complex nanophotonic properties of the nanostructured layer stack of the ITO front electrode and the adjacent layers. We can picture these nanophotonic properties in two macroscopic effects: (i) an effective match of the refractive index due to the dimensions of the nanostructures below the wavelength of incident light and (ii) parts of the light reflected at the nanopatterned electrode are diffracted at the two-dimensional grating texture beyond the angle of total internal refraction of the front glass/air interface. The combined effects ensure that incident light is transmitted with reduced parasitic reflection losses into the photo-active perovskite layer.

Having shown that the absorptance of perovskite solar cells with nanophotonic front electrodes is enhanced, the arising question is to which extent this enhancement leads to enhanced photocurrent generation, i.e., power conversion efficiency η. To answer this question and spectrally resolve the effect, we compare the external quantum efficiency *EQE* of the solar cells deposited on the nanophotonic front electrode (with periods of 500 nm and 800 nm) to the solar cell prepared on the flat reference front electrode (cf. Figure 2(e)). At very short wavelengths below 400 nm, the parasitic losses in the ITO front electrode are known to dominate the absorptance of the device such that the *EQE* is reduced. For wavelengths longer than 800 nm, the EQE vanishes since no light can be absorbed in the perovskite layer above its band gap of 1.55 eV. For wavelength between 400 nm and 750 nm, the *EQE* shows a similar trend compared to the absorptance, i.e., the *EQE* is enhanced in this wavelength region for the solar cells prepared on the nanophotonic front electrodes. Moreover, the enhancement in *EQE* is maximum for the nanophotonic front electrodes with 500 nm period of the nanopatterns, which also showed the strongest enhancement in absorptance (cf. Figure 2(d)). From the *EQE*, the short-circuit current density J_{SC} of the solar cells is derived under consideration of the AM1.5 spectrum. We find that the best nanophotonic ITO front electrode shows 5% improvement in J_{SC} compared to the flat reference due to reduced reflection of incident light at the front interfaces of the solar cell.

Importantly, the enhancement in J_{SC} also leads to an improved initial power conversion efficiency η of 9.9% compared to 9.6% for the solar cells prepared on the nanophotonic front electrode and the flat electrode, respectively. This relative improvement of 3% in η is less than the relative improvement of 5% in J_{SC}, since a slight decrease in fill factor *FF* is observed, while comparable open-circuit voltages V_{OC} are obtained (see Table I). Our prototype irrevocably demonstrates that solution-processed methylammonium lead iodide perovskite solar cells of very comparable electrical properties can be fabricated on flat ITO electrodes and nanopatterned ITO front electrodes with moderate aspect ratio of the nanostructures. The shallow design of the used transparent and conductive nanostructures enabled easy integration into our solution-based processing of the solar cell. It shall be noted that power conversion efficiencies of up to 14.2% have been realized on flat commercialized ITO substrates for the given device architecture. However, due to reduced transmittance, reduced conductivity, and increased roughness of our in-house ITO, the efficiency of the flat reference ITO decreased significantly.

To validate our interpretation of the improved light incoupling at the nanophotonic ITO front electrode in methylammonium lead iodide perovskite solar cells, we perform

TABLE I. Solar cell parameters. Fill factor *FF*, open-circuit voltage V_{OC}, short-circuit current density J_{SC}, and the power conversion efficiency η of the methylammonium lead iodide solar cells fabricated on a flat electrode and nanophotonic electrodes with a period, *p*, of 500 nm and 1000 nm.

ITO electrode	*FF*	V_{OC} (V)	J_{SC} (mA/cm^2) (*calc. from EQE*)	η (%)
Flat	0.59	0.89	18.3	9.6
Nanophotonic (p = 500 nm)	0.59	0.87	19.4	9.9
Nanophotonic (p = 1000 nm)	0.57	0.88	18.5	9.3

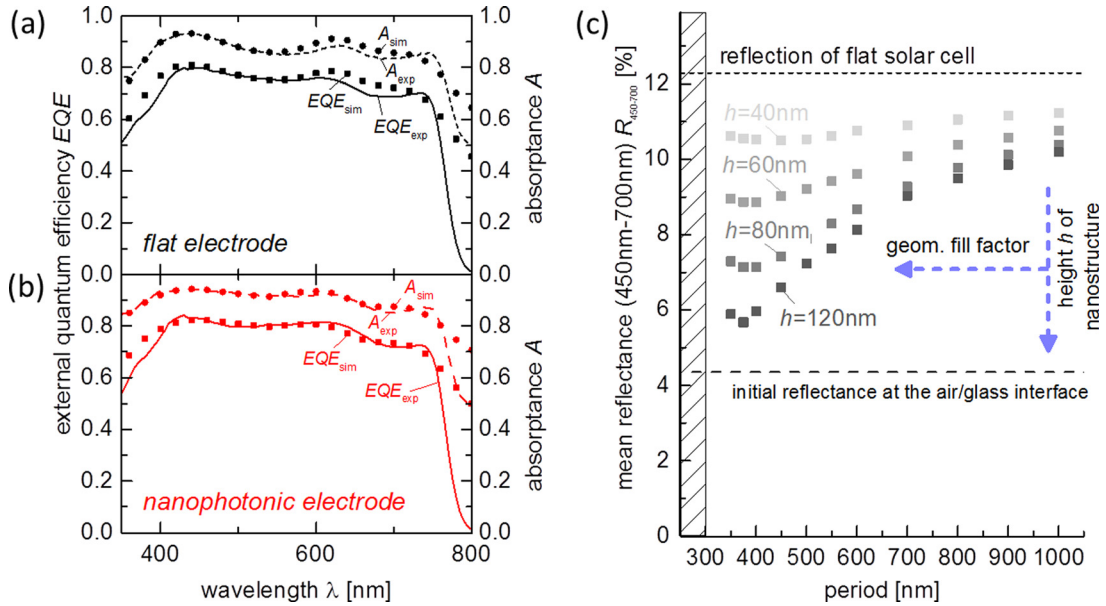

FIG. 3. Numerical simulations. (a) Comparison of simulated absorptance A_{sim} and measured absorptance A_{exp}, as well as simulated external quantum efficiency EQE_{sim} and measured EQE_{exp} of methylammonium lead iodide solar cell with flat ITO front electrode. (b) The same comparison but for a nanophotonic ITO front electrode (period 500 nm). (c) Simulated average reflectance (for $350 < \lambda < 750$ nm) for nanophotonic electrodes with various heights of the nanopattern and various periods.

three-dimensional electromagnetic simulations of solar cells with flat and with nanophotonic ITO front electrodes. From the simulated electromagnetic field distribution, we derive the total absorptance of the solar cell and the absorptance in the photo-active perovskite layer. The thicknesses of the layers are taken from profilometer measurements and the geometry of the nanopatterns are taken from AFM images (Figure 2(c)). To simplify the geometry, we assumed a cubic nanostructure of the nanopatterns on the resist (height 80 nm, width 300 nm) and semi-ellipsoidal nanostructures (height 80 nm, width 320 nm) at the surface of the ITO. The optical data of the perovskite material is taken from ellipsometry measurements of bare perovskite films (details in the supplementary material[36]). Our simulations show a convincing agreement between simulated and measured absorptance with flat and with nanophotonic ITO front electrodes (see Figure 3(a)). Moreover, assuming charge carrier collection efficiency (viz., internal quantum efficiency) of 90% in the photoactive perovskite layer, we obtain a simulated *EQE* that matches well the measured *EQE* of the solar cells with flat and nanophotonic electrode (see Figure 3(b)). These agreements demonstrate the relevance and predictive power of our simulations. Most importantly, our simulations prove that the nanopatterns of the front electrodes induce improved light incoupling that accounts for the reduced parasitic reflection.

Having proven that the simulated reflectance and *EQE* are in good agreement with the measured data of the prototype solar cells, we numerically investigate the dependence of the light management of the nanophotonic ITO front electrode on the geometry of the nanopattern. In Figure 3(c), the simulated average reflectance $\langle R \rangle_{450-700}$ (for $400\,\text{nm} < \lambda < 700\,\text{nm}$) is shown for periods of the nanopattern from 400 nm to 1200 nm and height of the nanostructures of 20 nm, 40 nm, 80 nm, and 120 nm. Two fundamental relations are validated: (i) the broad band reflectance decreases with increasing geometrical fill factor of the nanostructures (i.e., decreasing period) until a minimum reflectance at periods around 350–400 nm and (ii) the broad band reflectance decreases with increasing height of nanostructures. These fundamental relations have been thoroughly studied for multiple applications of anti-reflection coatings.[27] The simulations show that improved geometries of the nanopatterns of ITO electrodes bear the potential to further decrease the reflectance losses. For example, half-ellipsoidal nanostructures with a base-diameter of 320 nm (as applied in this contribution) with periods of 400 nm and a height of 120 nm leads to broad band reflectance of 5.7%. This broad band reflectance is already very close to the minimum broad band reflectance of around 4.3% given by the planar air/glass interface. In future studies, the shape, unit cell, and dielectric layer stack of the nanophotonic front electrode will be optimized to further reduce the reflectance losses. Foreseen strategies to further decrease the reflection are nanopatterns with increasing geometrical fill factor of the nanostructures (decreasing period, hexagonal unit cell), an increasing height, and a more tapered shape of the nanostructures. These strategies will enable a further improved transmission at the interfaces of perovskite solar cells. The applied UV-nanoimprint process shown here is capable of replication at precision down to a few nanometers, including random textures and high aspect ratios periodic nanopatters.[40–43]

The presented nanophotonic front electrodes for improved broad band light transmittance into the solar cell can also be applied for improved light transmittance at the rear side of the perovskite solar cell. Such functionality is highly desired in the long wavelength range for tandem device concepts with perovskite solar cell.[15,44,45] Similar nanopatterns to those investigated in this contribution have already been replicated into transparent substrates on large scale for photovoltaic applications at low costs.[46] Thus, the industrial realization of our nanophotonic front electrode for improved light incoupling in perovskite solar cells is in reach.

In conclusion, we present a versatile, large-area applicable nanophotonic front electrode for application in perovskite solar cells. The nanopatterns of the nanophotonic ITO electrode reduce the parasitic reflectance losses by effectively matching the refractive indices of the layers at the front side of the solar cell. Our prototype methylammonium lead iodide perovskite solar cell shows an relative improvement of 5% in short-circuit current density and a power conversion efficiency improvement from 9.6% to 9.9% compared to the flat reference device.

The authors thank Erwin Vandenplas, M. Smeets, Manuela Meier, and A. Schmalen for the technical support. The fruitful discussions with M. Meier, T. Kirchartz, U. Rau, J. Tait, J. Bastos, E. Voroshazi, and A. Hadipour are highly appreciated. This research has received (partial) funding from the Flemish Government—Department of Economics, Science and Innovation as well as the European Commission's Seventh Framework Program (Mujulima 604148). The work of Ulrich W. Paetzold was financed by the PostDoc Program of the German Academic Exchange Program (DAAD).

[1]H.-S. Kim, C.-R. Lee, J.-H. Im, K.-B. Lee, T. Moehl, A. Marchioro, S.-J. Moon, R. Humphry-Baker, J.-H. Yum, J. E. Moser, M. Grätzel, and N.-G. Park, Sci. Rep. **2**, 591 (2012).
[2]Research Cell Efficiency Records see http://www.nrel.gov/ncpv/.
[3]N.-G. Park, Mater. Today **18**(2), 65 (2014).
[4]H. Zhou, Q. Chen, G. Li, S. Luo, T. -b. Song, H.-S. Duan, Z. Hong, J. You, Y. Liu, and Y. Yang, Science **345**, 542 (2014).
[5]A. Mei, X. Li, L. Liu, Z. Ku, T. Liu, Y. Rong, M. Xu, M. Hu, J. Chen, Y. Yang, M. Gratzel, and H. Han, Science **345**, 295 (2014).
[6]G. Niu, W. Li, F. Meng, L. Wang, H. Dong, and Y. Qiu, J. Mater. Chem. A **2**, 705 (2014).
[7]J. Burschka, N. Pellet, S.-J. Moon, R. Humphry-Baker, P. Gao, M. K. Nazeeruddin, and M. Grätzel, Nature **499**, 316 (2013).
[8]S. A. Bretschneider, J. Weickert, J. A. Dorman, and L. Schmidt-Mende, APL Mater. **2**, 040701 (2014).
[9]H. J. Snaith, A. Abate, J. M. Ball, G. E. Eperon, T. Leijtens, N. K. Noel, S. D. Stranks, J. T. Wang, K. Wojciechowski, and W. Zhang, J. Phys. Chem. Lett. **5**, 1511 (2014).
[10]N. K. Noel, S. D. Stranks, A. Abate, C. Wehrenfennig, S. Guarnera, A.-A. Haghighirad, A. Sadhanala, G. E. Eperon, S. K. Pathak, M. B. Johnston, A. Petrozza, L. M. Herz, and H. J. Snaith, Energy Environ. Sci. **7**, 3061 (2014).
[11]F. Hao, C. C. Stoumpos, D. H. Cao, R. P. H. Chang, and M. G. Kanatzidis, Nature Photon. **8**, 489 (2014).
[12]G. Xing, N. Mathews, S. Sun, S. S. Lim, Y. M. Lam, M. Grätzel, S. Mhaisalkar, and T. C. Sum, Science **342**, 344 (2013).
[13]S. D. Stranks, G. E. Eperon, G. Grancini, C. Menelaou, M. J. P. Alcocer, T. Leijtens, L. M. Herz, A. Petrozza, and H. J. Snaith, Science **342**, 341 (2013).
[14]S. De Wolf, J. Holovsky, S.-J. Moon, P. Löper, B. Niesen, M. Ledinsky, F.-J. Haug, J.-H. Yum, and C. Ballif, J. Phys. Chem. Lett. **5**, 1035 (2014).
[15]H. J. Snaith, J. Phys. Chem. Lett. **4**, 3623 (2013).
[16]O. Malinkiewicz, A. Yella, Y. H. Lee, G. M. Espallargas, M. Graetzel, M. K. Nazeeruddin, and H. J. Bolink, Nature Photon. **8**, 128 (2013).
[17]M. Grätzel, Nat. Mater. **13**, 838 (2014).
[18]M. A. Green, A. Ho-Baillie, and H. J. Snaith, Nature Photon. **8**, 506 (2014).
[19]C. Wehrenfennig, G. E. Eperon, M. B. Johnston, H. J. Snaith, and L. M. Herz, Adv. Mater. **26**, 1584 (2014).
[20]Y. Takahashi, R. Obara, Z.-Z. Lin, Y. Takahashi, T. Naito, T. Inabe, S. Ishibashi, and K. Terakura, Dalton Trans. **40**, 5563 (2011).
[21]M. Liu, M. B. Johnston, and H. J. Snaith, Nature **501**, 395 (2013).
[22]M. M. Lee, J. Teuscher, T. Miyasaka, T. N. Murakami, and H. J. Snaith, Science **338**, 643 (2012).
[23]Q. Chen, H. Zhou, Z. Hong, S. Luo, H. Duan, H. Wang, Y. Liu, G. Li, and Y. Yang, J. Am. Chem. Soc. **136**, 622 (2014).
[24]L. Zhu, J. Xiao, J. Shi, J. Wang, S. Lv, Y. Xu, Y. Luo, Y. Xiao, S. Wang, Q. Meng, X. Li, and D. Li, "Efficient $CH_3NH_3PbI_3$ perovskite solar cells with 2TPA-*n*-DP hole-transporting layers," Nano Res. (published online).
[25]J. H. Heo, S. H. Im, J. H. Noh, T. N. Mandal, C. Lim, J. A. Chang, Y. H. Lee, H. Kim, A. Sarkar, M. K. Nazeeruddin, M. Grätzel, and S. Il Seok, Nature Photon. **7**, 486 (2013).
[26]W. Jaegermann, A. Klein, and T. Mayer, Adv. Mater. **21**, 4196 (2009).
[27]H. K. Raut, V. A. Ganesh, A. S. Nair, and S. Ramakrishna, Energy Environ. Sci. **4**, 3779 (2011).
[28]S. Y. Chou and W. Ding, Opt. Express **21**(Suppl 1), A60 (2013).
[29]D.-H. Ko, J. R. Tumbleston, A. Gadisa, M. Aryal, Y. Liu, R. Lopez, and E. T. Samulski, J. Mater. Chem. **21**, 16293 (2011).
[30]D. H. Wang, D.-G. Choi, K.-J. Lee, J.-H. Jeong, S. H. Jeon, O. O. Park, and J. H. Park, Org. Electron. **11**, 285 (2010).
[31]C. Battaglia, C.-M. Hsu, K. Söderström, J. Escarré, F.-J. Haug, M. Charrière, M. Boccard, M. Despeisse, D. T. L. Alexander, M. Cantoni, Y. Cui, and C. Ballif, ACS Nano **6**, 2790 (2012).
[32]U. W. Paetzold, M. Smeets, M. Meier, K. Bittkau, T. Merdzhanova, V. Smirnov, D. Michaelis, C. Waechter, R. Carius, and U. Rau, Appl. Phys. Lett. **104**, 131102 (2014).
[33]K. S. Cho, P. Mandal, K. Kim, I. H. Baek, S. Lee, H. Lim, D. J. Cho, S. Kim, J. Lee, and F. Rotermund, Opt. Commun. **284**, 2608 (2011).
[34]P. Bermel, C. Luo, L. Zeng, L. C. Kimerling, and J. D. Joannopoulos, Opt. Express **15**, 16986 (2007).
[35]C. Trompoukis, O. El Daif, V. Depauw, I. Gordon, and J. Poortmans, Appl. Phys. Lett. **101**, 103901 (2012).
[36]See supplementary material at http://dx.doi.org/10.1063/1.4918751 for details on the fabrication of nanophotonic front electrodes, fabrication of the perovskite solar cells, and characterization techniques.
[37]M. Meier, U. W. Paetzold, M. Prömpers, T. Merdzhanova, R. Carius, and A. Gordijn, Prog. Photovoltaics: Res. Appl. **22**, 1226 (2013).
[38]U. W. Paetzold, W. Zhang, M. Prömpers, J. Kirchhoff, T. Merdzhanova, S. Michard, R. Carius, A. Gordijn, and M. Meier, Mater. Sci. Eng. B **178**, 617 (2013).
[39]S. Bai, Z. Wu, X. Wu, Y. Jin, N. Zhao, Z. Chen, Q. Mei, X. Wang, Z. Ye, T. Song, R. Liu, S. Lee, and B. Sun, Nano Res. **7**, 1749 (2014).
[40]H. Schift, J. Vac. Sci. Technol. B: Microelectron. Nanometer Struct. **26**, 458 (2008).
[41]S. Y. Chou, P. R. Krauss, and P. J. Renstrom, Science **272**, 85 (1996).
[42]J. Escarré, K. Söderström, C. Battaglia, F. Haug, and C. Ballif, Sol. Energy Mater. Sol. Cells **95**, 881 (2011).
[43]E. A. Costner, M. W. Lin, W. Jen, and C. G. Willson, Annu. Rev. Mater. Res. **39**, 155 (2009).
[44]B. W. Schneider, N. N. Lal, S. Baker-Finch, and T. P. White, Opt. Express **22**, A1422 (2014).
[45]P. Loper, B. Niesen, S.-J. Moon, S. Martin de Nicolas, J. Holovsky, Z. Remes, M. Ledinsky, F.-J. Haug, J.-H. Yum, S. De Wolf, and C. Ballif, IEEE J. Photovolt. **4**, 1545 (2014).
[46]A. J. M. van Erven, M. Steltenpool, M. Bos, J. Rutten, G. van der Hofstad, J. Muller, H. de Groot, J. de Ruijter, A. Tavakoliyaraki, B. Titulaer, and G. Rajeswaran, in *2012 38th IEEE Photovoltaic Specialists Conference* (IEEE, 2012), pp. 000690–000693.